AD_____

Award Number: W81XWH-05-1-0480

TITLE: In Vivo Molecular Imaging of Mammary Tumorigenesis in Murine Model Systems

PRINCIPAL INVESTIGATOR: Margaret S. Saha, Ph.D.

CONTRACTING ORGANIZATION: College of William and Mary
Williamsburg, VA 23187

REPORT DATE: August 2006

TYPE OF REPORT: Annual

PREPARED FOR: U.S. Army Medical Research and Materiel Command
Fort Detrick, Maryland 21702-5012

REPORT DOCUMENTATION PAGE

Form Approved
OMB No. 0704-0188

1. REPORT DATE *(DD-MM-YYYY)*	**2. REPORT TYPE**	**3. DATES COVERED** *(From - To)*
01-08-2006	Annual	1 AUG 2005 - 31 JUL 2006

4. TITLE AND SUBTITLE
In Vivo Molecular Imaging of Mammary Tumorigenesis in Murine Model Systems

5a. CONTRACT NUMBER

5b. GRANT NUMBER
W81XWH-05-1-0480

5c. PROGRAM ELEMENT NUMBER

6. AUTHOR(S)
Margaret S. Saha, Ph.D.

E-Mail: mssaha@wm.edu

5d. PROJECT NUMBER

5e. TASK NUMBER

5f. WORK UNIT NUMBER

7. PERFORMING ORGANIZATION NAME(S) AND ADDRESS(ES)

College of William and Mary
Williamsburg, VA 23187

8. PERFORMING ORGANIZATION REPORT NUMBER

9. SPONSORING / MONITORING AGENCY NAME(S) AND ADDRESS(ES)
U.S. Army Medical Research and Materiel Command
Fort Detrick, Maryland 21702-5012

10. SPONSOR/MONITOR'S ACRONYM(S)

11. SPONSOR/MONITOR'S REPORT NUMBER(S)

12. DISTRIBUTION / AVAILABILITY STATEMENT
Approved for Public Release; Distribution Unlimited

13. SUPPLEMENTARY NOTES

14. ABSTRACT:

The development of accurate diagnostic tools and effective breast cancer treatments requires the ability to detect the presence of pre-cancerous, cancerous, and metastatic tissue and to identify the particular subtype or class of tumor. It is equally imperative to develop the capability of performing a "molecular diagnosis" non-invasively, employing *in vivo* imaging technologies in order to follow the tumor progression over time. This project entails an interdisciplinary approach which employs a gamma-ray-camera detector system to follow, during tumorigenesis, the uptake of NaI through the Na+/I- symporter, and the binding characteristics and localization of vascular endothelial growth factor, epidermal growth factor, and estradiol in mouse models of breast cancer. Using the MMTV model for mammary tumor development, we have found that I-125 labeled sodium iodide provides a valuable tag for imaging mammary tumors at several different stages of their development. Moreover, it is also able to provide an image of the heterogeneity among tumors and within a given tumor, making it potentially useful as a strategy for non-invasively imaging and classifying mammary tumors for purposes of prognosis.

15. SUBJECT TERMS
Mammary tumor; in vivo; imaging; breast cancer; mouse models

16. SECURITY CLASSIFICATION OF:			**17. LIMITATION OF ABSTRACT**	**18. NUMBER OF PAGES**	**19a. NAME OF RESPONSIBLE PERSON**
a. REPORT	**b. ABSTRACT**	**c. THIS PAGE**			USAMRMC
U	U	U	UU	23	**19b. TELEPHONE NUMBER** *(include area code)*

Standard Form 298 (Rev. 8-98)
Prescribed by ANSI Std. Z39.18

Table of Contents

INTRODUCTION

The development of accurate diagnostic tools and effective breast cancer treatments requires the ability to detect the presence of pre-cancerous, cancerous, and metastatic tissue and to identify the particular subtype or class of tumor. It is equally imperative to develop the capability of performing a "molecular diagnosis" non-invasively, employing *in vivo* imaging technologies in order to follow the tumor progression over time. This project entails an interdisciplinary approach which employs a gamma-ray-camera detector system to follow, during tumorigenesis, the uptake of NaI through the Na+/I- symporter (Cho, 2002; Chung, 2003: Dadachova and Carrasco, 2004; Dadachova and Zuckier, 2003) and the binding characteristics and localization of vascular endothelial growth factor, epidermal growth factor, and estradiol. All of these molecules have been implicated as key players in the oncogenesis in breast cancer. Using a dual modality (gamma and x-ray) small animal detector system (H8500 Hamamatsu position sensitive photomultiplier tubes and a pixelated NaI(Tl) crystal array with a CuBe parallel-hole collimator), these radioactively tagged molecules will be imaged over time in the same animal using three mouse models of breast cancer: mouse mammary tumor virus mice, HER2/neu transgenic mice, and PyMT (polyoma middle T antigen) transgenic mice. In addition, these *in vivo* data will be correlated with results obtained from gene expression studies using RT-PCR analysis. Combining *in vivo* molecular imaging with gene expression technology will allow for merging of diverse data sets to establish potentially novel correlations as well as the ability to compare and validate results with gene expression profiles from human data sets.

BODY OF REPORT

As specified in our Statement of Work document the past year has focused on (1) making our detector system functional for the imaging of mammary tumors; (2) using the MMTV breast cancer tumor model to conduct an extensive series of imaging with I-125 labeled sodium iodide as well as TGF-alpha, estradiol and VEGF; (3) conduct an extensive series of analyses using the imaging data to draw conclusions regarding the use of these compounds as imaging agents for breast cancer; completed some of the molecular work linking the imaging data to the molecular events. A significant amount of effort has been devoted to the analysis of our data. We summarize progress on our project by describing the key issues which our work addressed in the past year.

Work conducted using I-125 NaI to image mammary tumors in MMTV tumor animals:

1. Number of tumor (MMTV) cases imaged and tumor distribution: overall statistics.

Excluding mice that were imaged for less than one hour, a total of 43 applicable mice were imaged including two mice imaged three times and five mice imaged twice. There is a total of 48 cases, nine of which are KI-blocked and should be separated from non-KI-blocked cases. Therefore, 39 MMTV cases were compared here. These cases include a total of 64 tumors, five of which were excluded from analysis because they were so close to thyroid that may cause huge errors in ROI. There were 59 comparable tumors remaining.

Tumor distribution: 22 tumors in left thorax, 23 in right thorax, four in left inguinal region, and 10 in right inguinal region. Tumors therefore develop in thorax region with a probability of ~76% (and ~ 24% in inguinal region), which means thorax tumors are more probable in MMTV mice.

2. Determination of the tumor size and the depth of heart (for future depth correction).

The depth of heart was based on the estimation and an actual measurement.

It is very challenging to determine the size of tumors precisely. However, the justification of tumor size is crucial because following ROI analysis is heavily based on it. Four steps were taken to precisely determine ROI and tumor size.

a. The tumor size was divided into three main categories: small, median, and large tumors. Each category includes three sub-divisions. Small tumors include small-1, small-2, and small-3 tumor. So do median and large tumors.
b. The tumors were sorted according to the size of a rectangular ROI called tumor-outer, which is used to cover the whole tumor as much as possible in ROI analysis.
c. Since the tumor-outer ROI always includes other tissues nearby the tumor more or less, visual correction was performed very carefully to finally determine the category to which the tumor belonged.
d. To obtain some idea of its physical size a small-1 size was regarded as a tumor with 4 mm diameter with an increment of 2 mm for subsequent tumor size based on the rough estimation using beads. The depth correction in following ROI analysis is based on this estimation.

The typical tumor size of the nine divisions is shown in following figures.

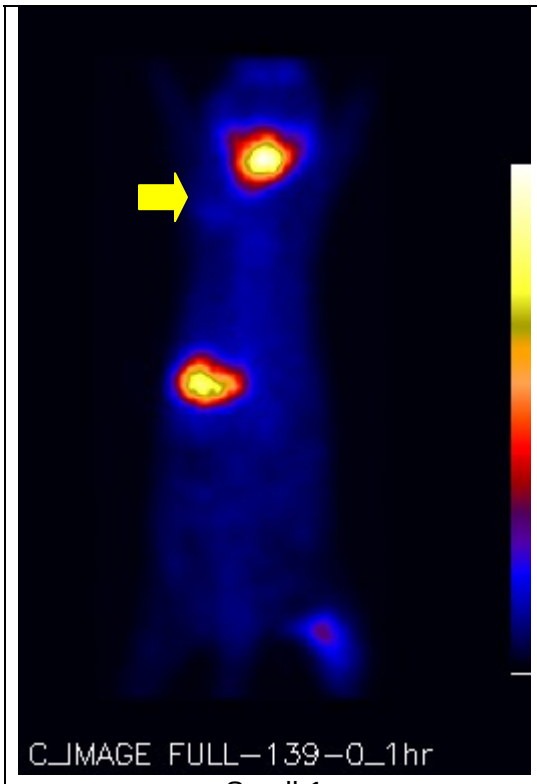

Small-1

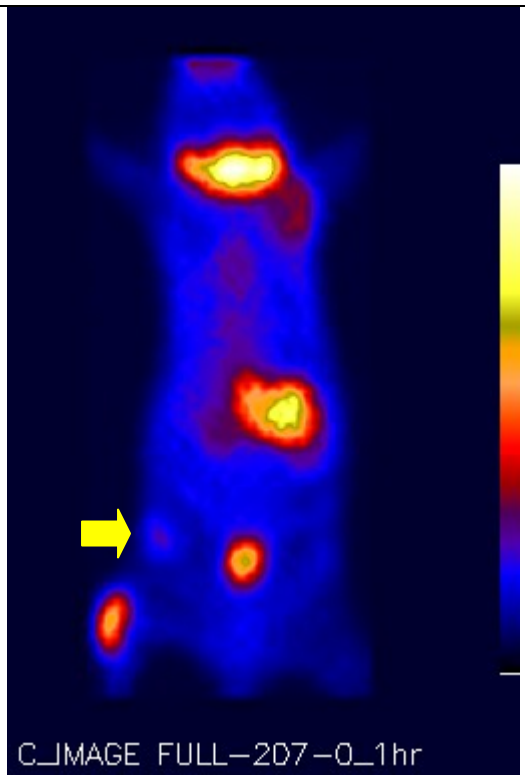

Small-2

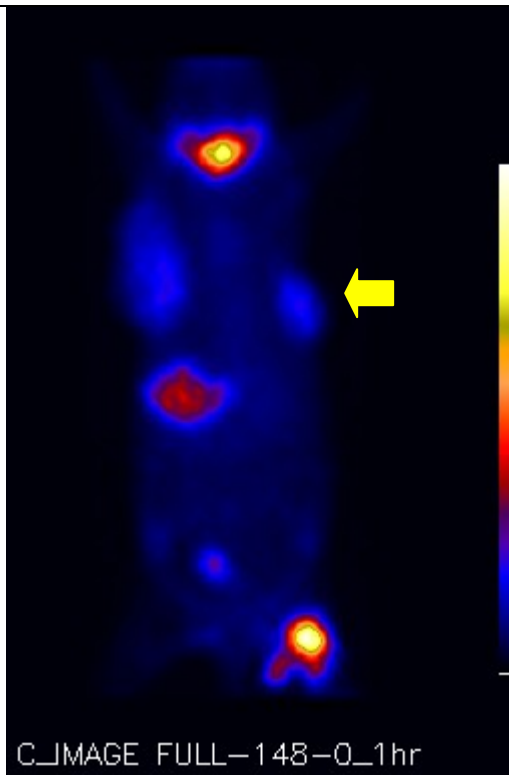

Small-3

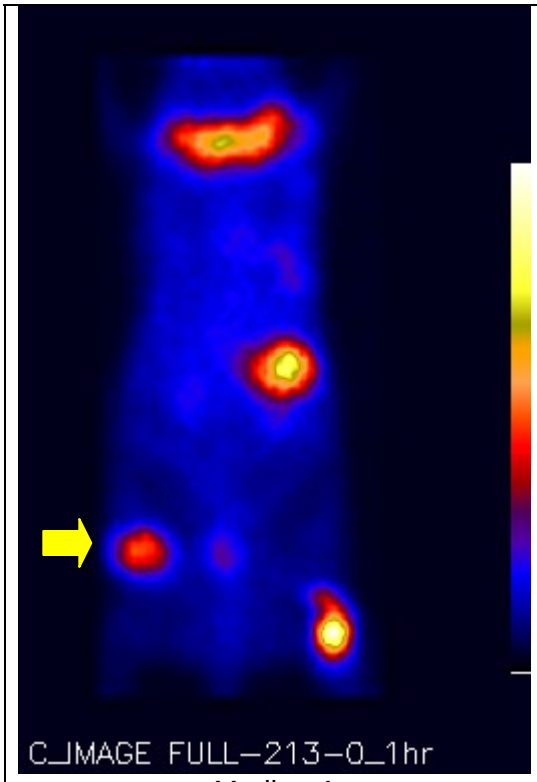

Median-1

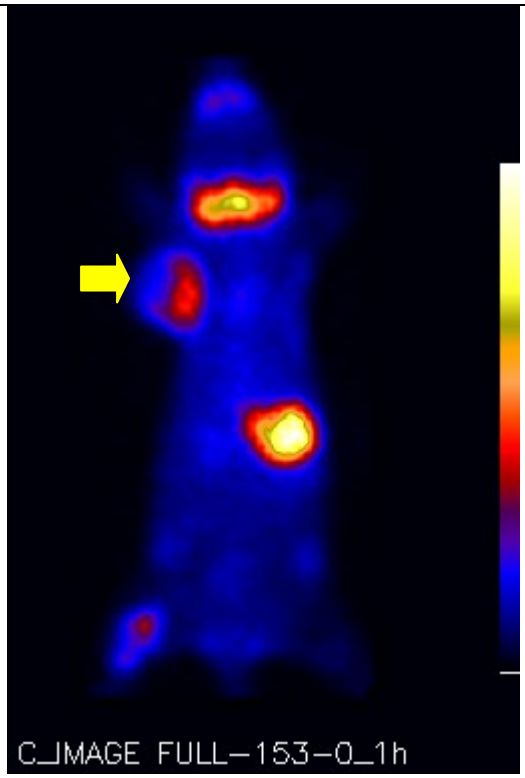

Median-2

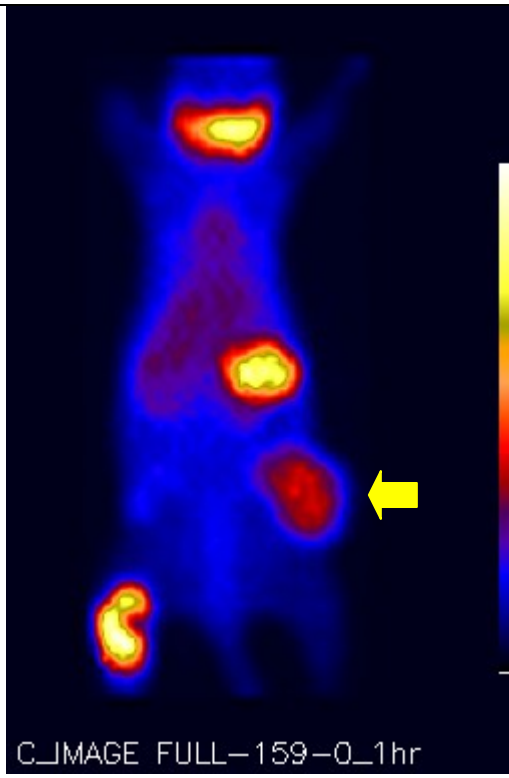

Median-3

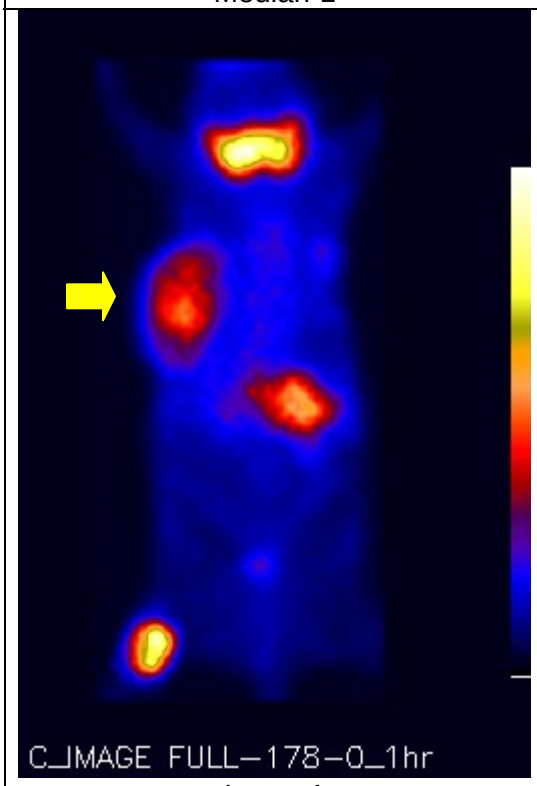

Large-1

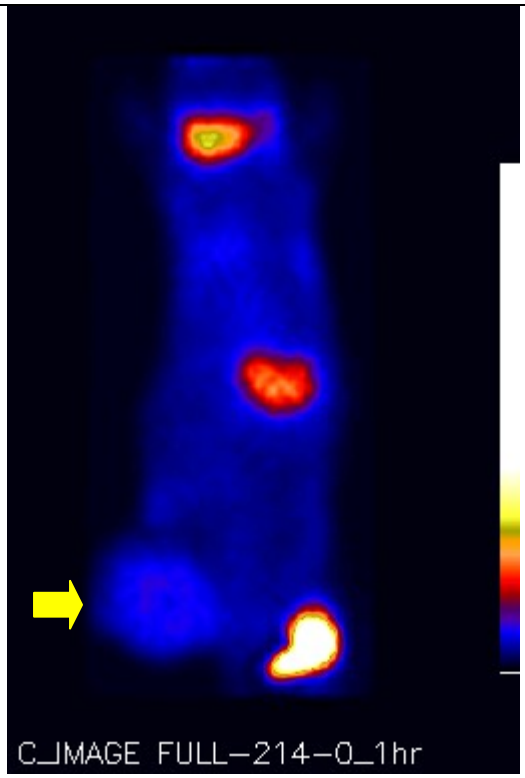

Large-2

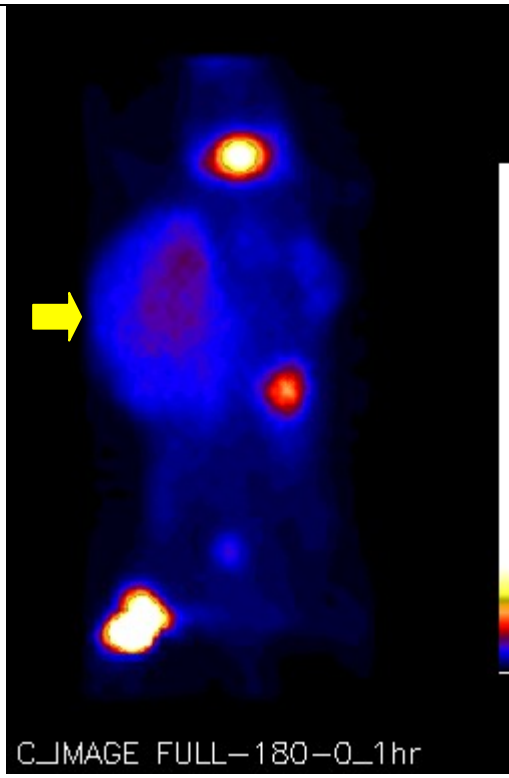

Advanced

3. Analysis of heart as a possible dynamic reference.

In order to learn whether the accumulation of isotope in a tumor or other tissues is simply blood flow, it is valuable to compare them with the heart, which is assumed to represent the isotope density in blood. A ratio of some organ/heart may reveal if only blood flow causes isotope uptake in that organ. On the other hand, heart as a dynamic reference may avoid the uncertainty of actually injected dose in a mouse. However, it was not clear whether using the heart as a dynamic reference is valid.

To address this question, the total counts of whole body, and the counts per pixel of heart and their ratio of all the MMTV cases (see the figures below) were summarized. These figures show that:

a. The counts in heart show a similar pattern corresponding to the body.
b. The heart/body ratio remains statistically constant (average is 0.000570973)

Based on the data, it appears that using the heart as a dynamic reference is valid. This was used in the following tumor analysis and compared with the data with body counts as a solid reference.

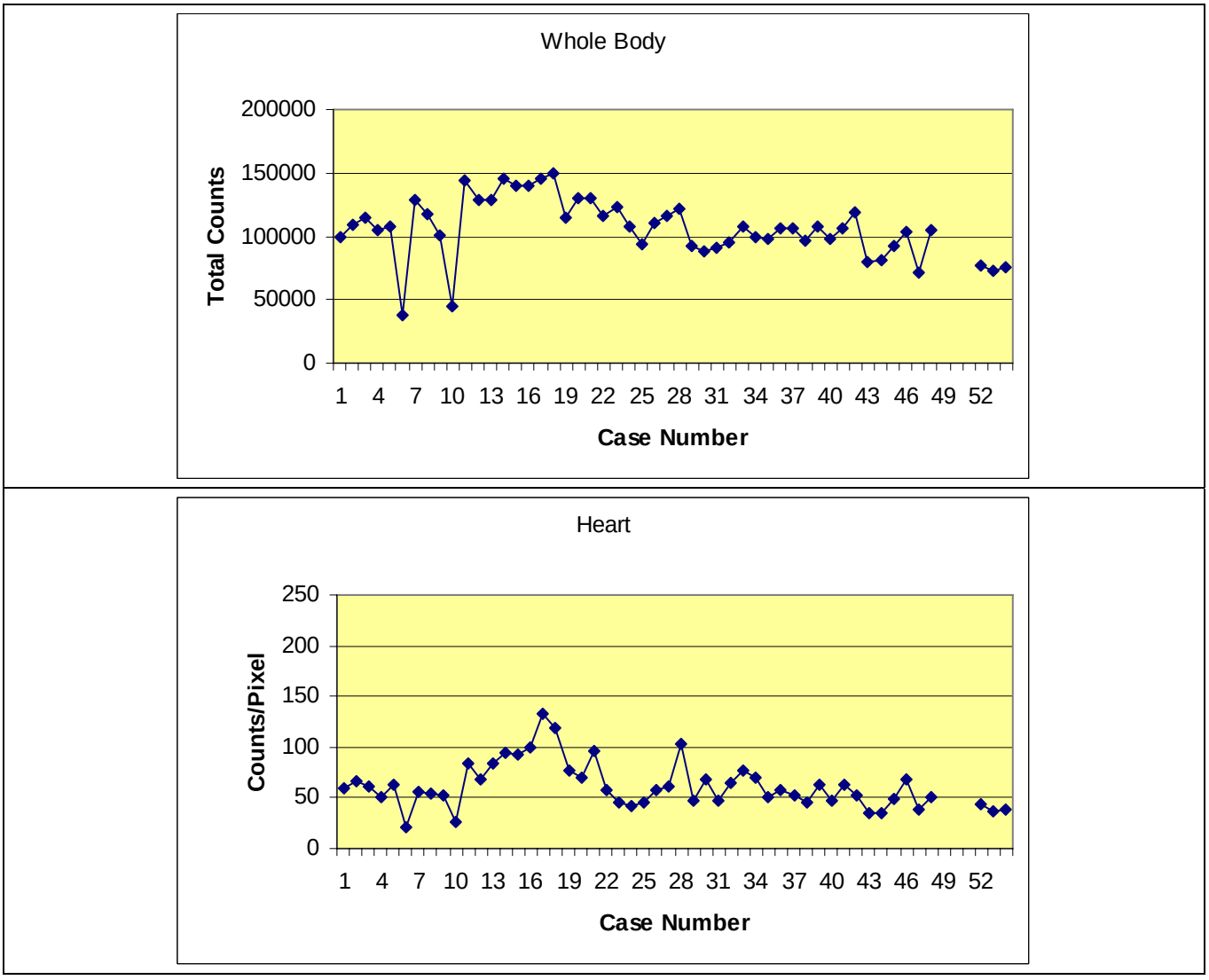

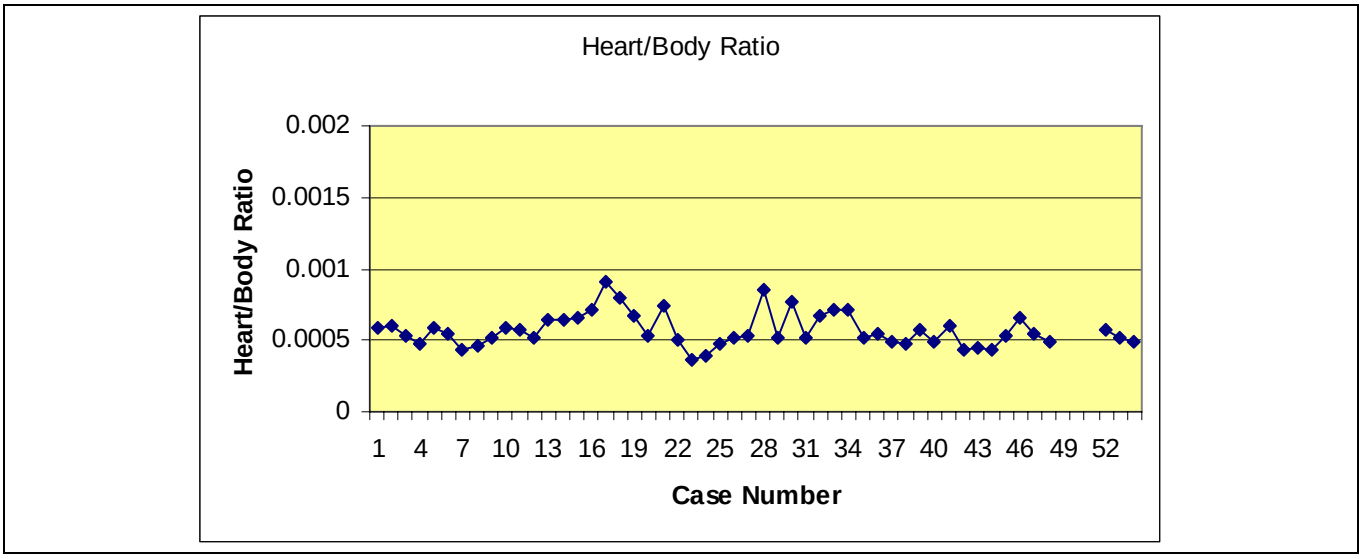

Subsequent analysis is based on the data of an averaged single pixel of the ROI applied for the hottest region of a tissue with/without depth correction if not specifically described. For the example of tumors, the averaged single pixel data of the hottest region (a 3x3 ROI) of a tumor vs. its size with/without depth correction was plotted.

4. Analysis and Interpretation of the raw ROI data of tumors.

The absolute counts per pixel of all the tumors and their averaged value are summarized below. It is important to note that the data will have meaning only if the injected dose represented by the total counts of the whole body (see previous figure) remains constant with acceptable variation. Depth correction was applied based on the estimation described above. Though less precise than the data using heart or body as a reference, these data are consistent with other data and suggest the following:

a. Without depth correction, the most active part of a tumor expresses increasing amounts of NIS activity as the tumor is becoming larger, which might suggest enhanced functions of tissues or growing tumor size. But accumulation levels off when the tumor becomes too large. It may mean the tumor tissue loses function. .

b. With depth correction, the tissue of a tumor presents strongest isotope uptake at its earliest stage and decrease as it grows.

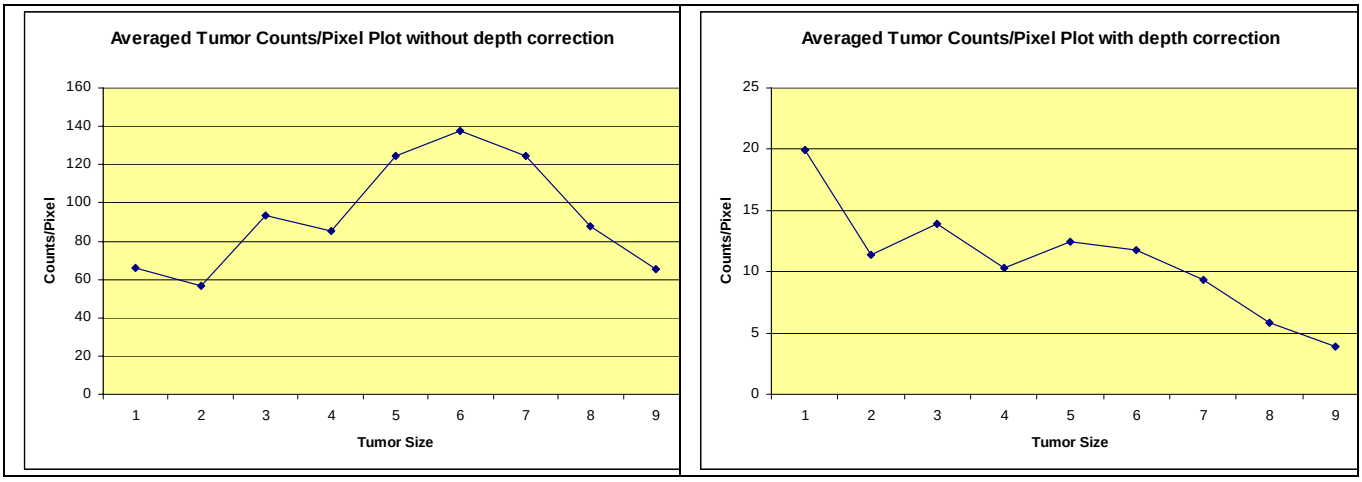

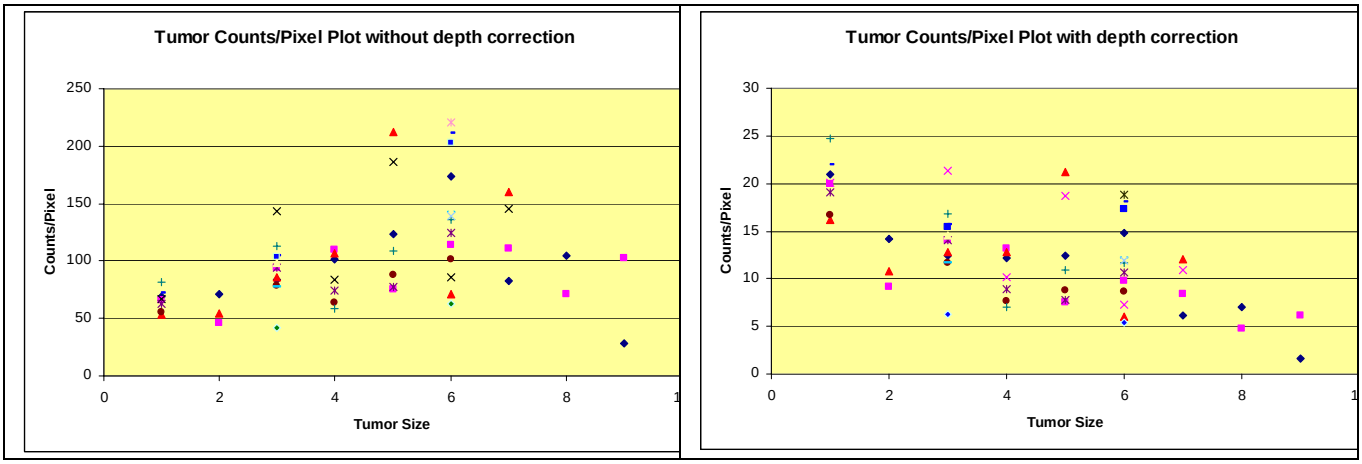

5. Analysis and interpretation of counts in the tumor/body ratio.

Comparison of tumor/body ratio should be much more precise than comparing the absolute ROI data of tumors because the variance of injection dose is taken into account. Those figures display generally the same conclusions as those summarized in point 4. Furthermore, it indicates:

a. Averaged median-2 (size 5) tumors express the strongest uptake (NIS activity, see Moon et al., 2001) in all the tumors WITHOUT depth correction. However, figures WITH depth correction imply that unit tissue of tumors in the earliest stage express the strongest NIS activity. Interestingly, the unit tumor tissue reached the second peak at median-2 size of tumor. It means that tumor at this stage is very active in NIS expression, which is noticeable both qualitatively and quantitatively.

b. Raw data in bottom two figures show that the majority of the tumors in early stages (small-1, -2 and -3) and advanced stages (large-2, advanced) have statistically identical amount of isotope uptake (NIS expression) respectively, which may mean similar pathology or physiology in the tumors at each stage. However, the tumors in middle stages (median-1,-2, -3, and large-1) present great variation and usually contain 2 or 3 group modes. This is very clear in size 5 (median-2) tumors. These tumors fall into two groups. This could be due to the different origins (the duct of a mammary gland vs. inside a mammary gland). It could also be due to the loss of functions of mammary glands caused by some of the developed tumors while other tumors may induce more NIS expression.

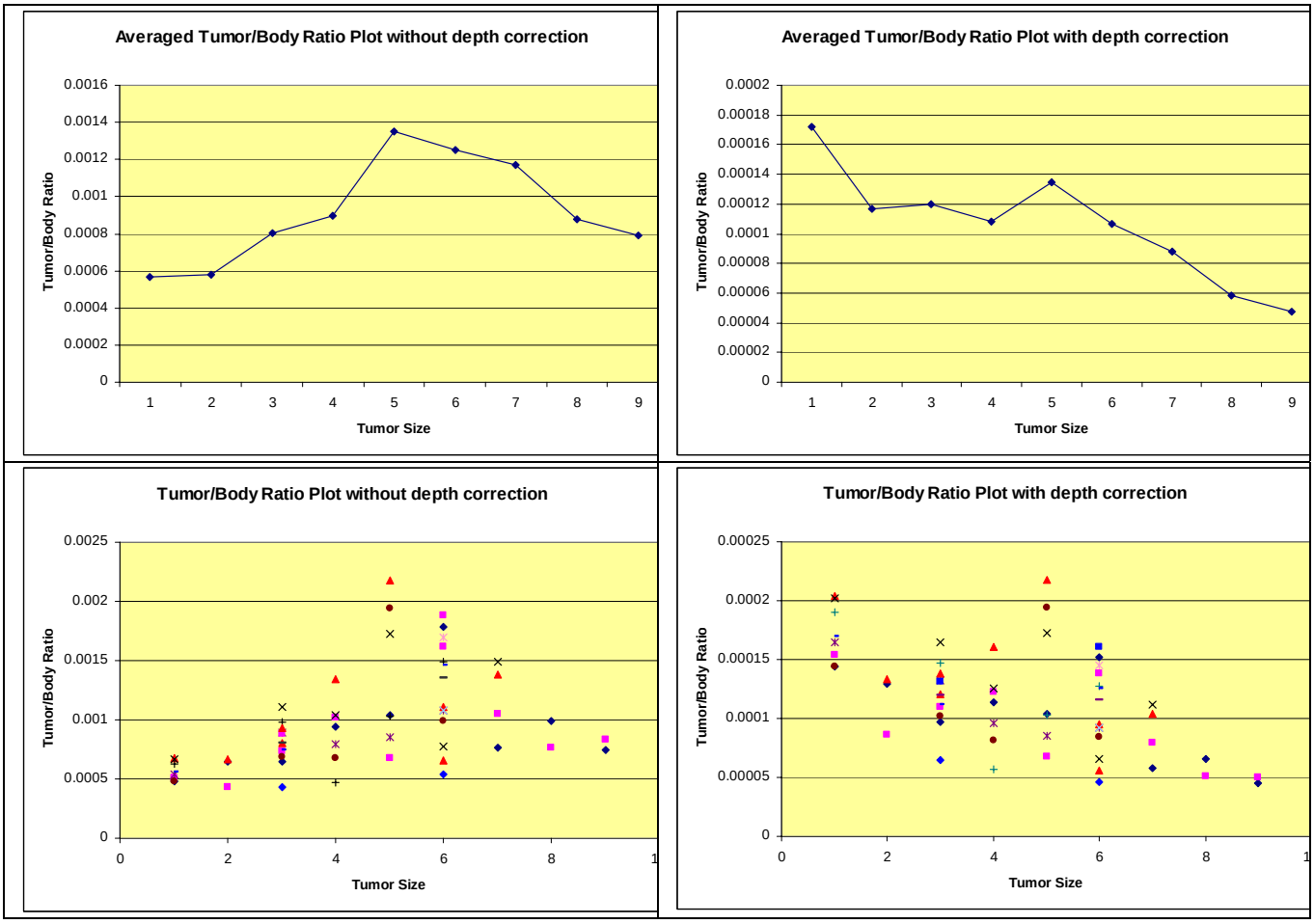

6. What do the figures of tumor/heart ratio mean?

Statistics based on raw data or tumor/body ratio can't unambiguously reveal if it's simply blood flow or isotope uptake/NIS expression that causes accumulation of isotopes in tumors. However, data of tumor/heart ratio make more sense if we agree that heart is qualified as blood flow and a dynamic reference. The following figures contain all the information consistent with item 5 except that the unit tumor tissue reached the second peak at median-1 tumors instead of median-2 tumors. Additionally, these data present that:

a. A ratio 1 in the plots WITHOUT depth correction means the whole tissue in the most active region of a tumor accumulates the isotope at the same level as the heart does. So the left plots display that all the tumors accumulate isotope at or above the level that a heart does except some of the smallest tumors.

b. A ratio less than 1 in the plots WITH depth correction means the isotope uptake is caused simply by blood flow. The average plot on the right indicates, overall, NIS expression happens in early stages of tumors (small and median size) until they developed into large tumors (large-1, 2 and advanced), where blood flow dominates the uptake of isotope.

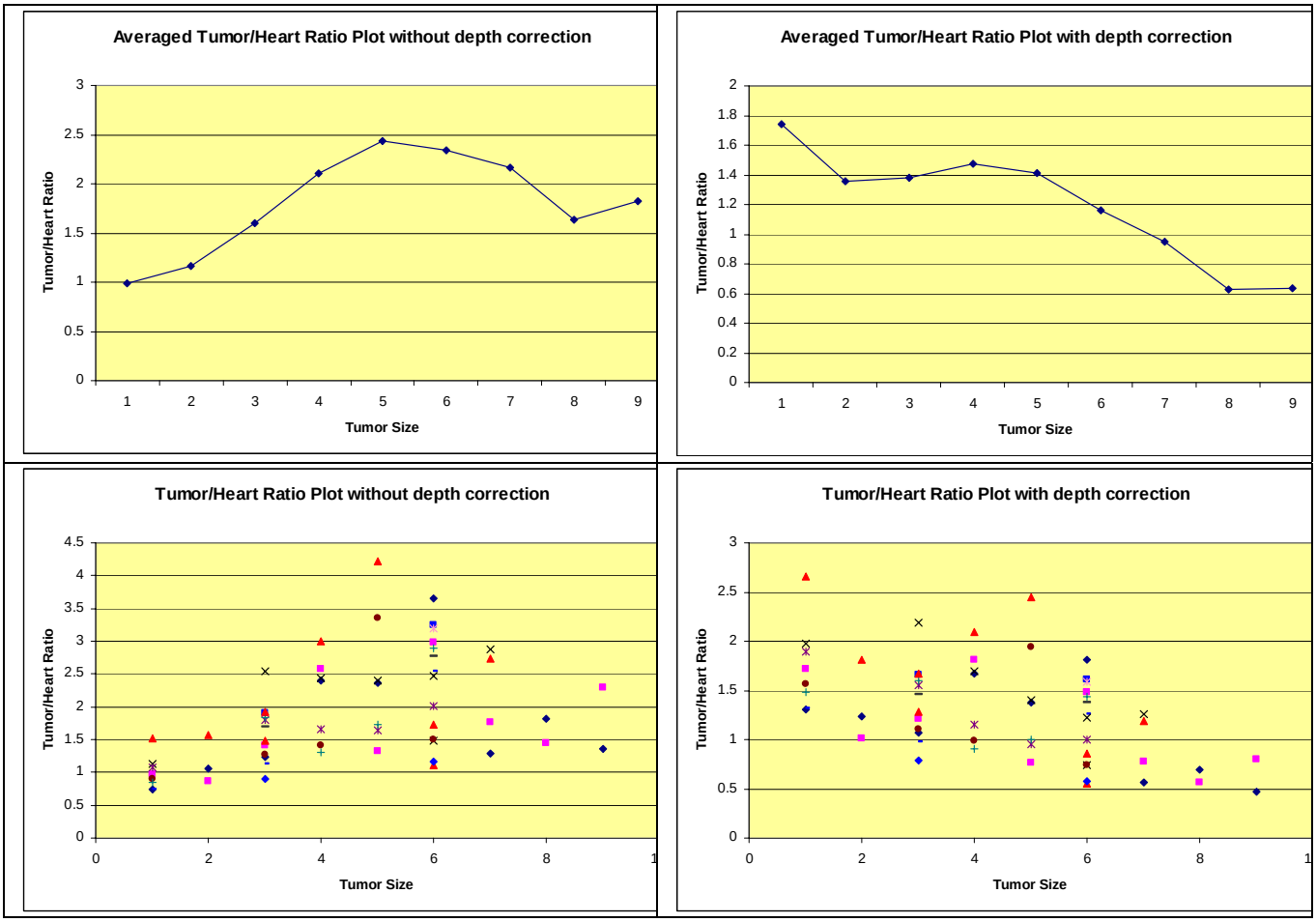

7. Analysis and interpretation of the normal mammary gland (NMG)/heart ratio and NMG/body ratio.

In ALMOST all the MMTV cases, some of the normal mammary glands (NMGs) were distinguished by increased uptake of isotope. This could be blood flow or NIS expression. To determine if existing tumors stimulate NIS expression in those NMGs, the hottest NMG of each mouse bearing tumor(s) were compared with the hottest NMGs of three MMTV mice which had no tumor at all. Initially we hypothesized that tumors stimulate NIS expression in NMGs. However, the data show it is a reverse case:

a. Pink dots in the figures below are NMGs of the mice without tumors. Even without depth correction, their ratios are above 1. Actually, if we assume a heart is 6 mm depth and a normal mammary gland is 2 mm thick, all the NMGs in the figure of NMG/heart ratio will have a ratio over 1 after depth correction, which implies all the NMGs have NIS expression beyond blood flow.

b. NMGs of the mice without tumors (pink dots) are obvious hotter than the majority of NMGs of the mice bearing tumors. It means that the existence of tumor may suppress the NIS expression in the latter.

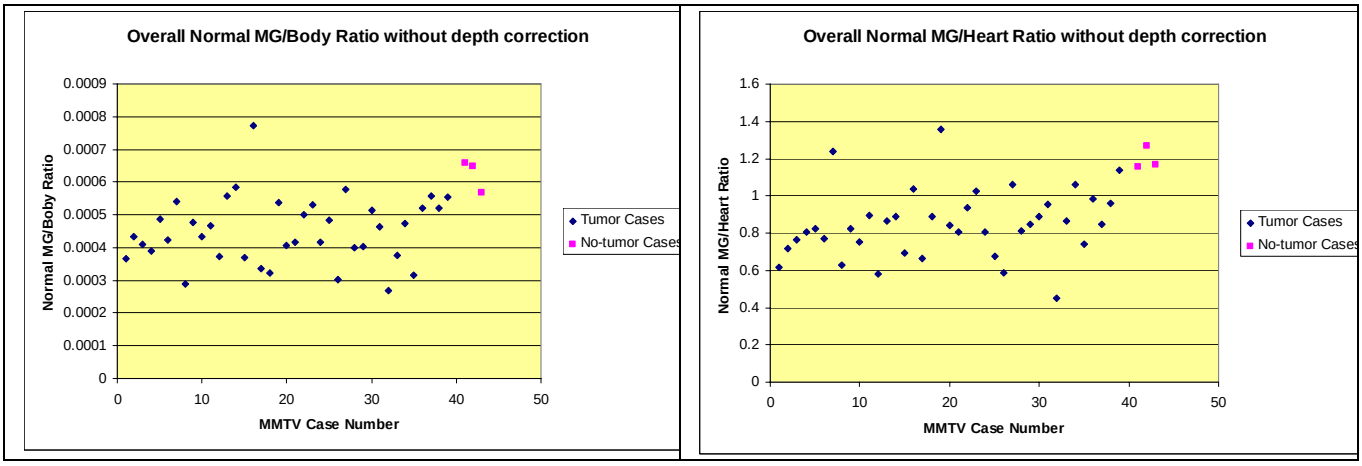

8. Analysis of two "references": leg background and heart and their change with time.

These are two references for investigators to determine the level the uptake of isotope in other tissues. The right column of figures is the averaged data of the left.

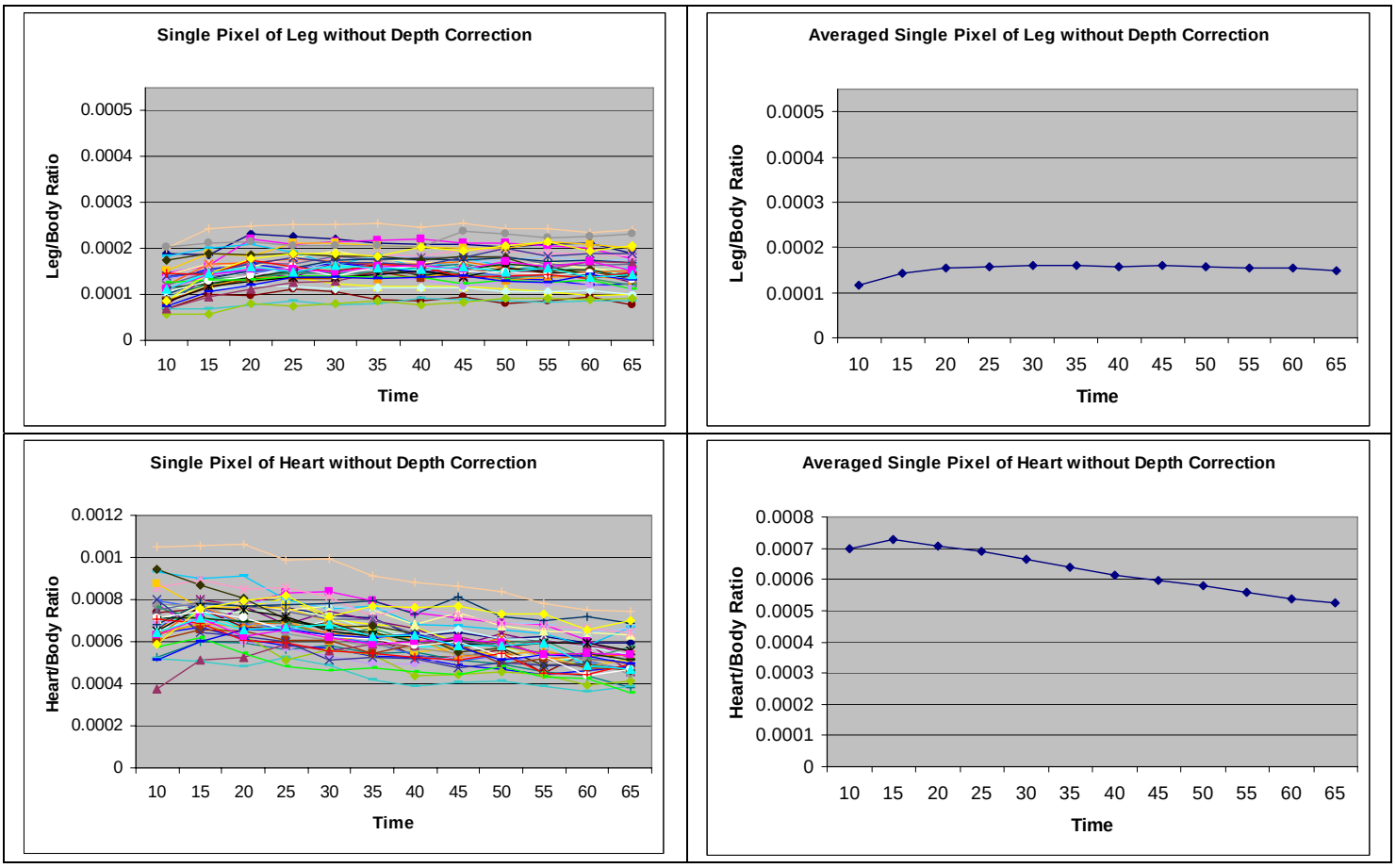

9. Analysis of isotope uptake/NIS activity of normal mammary glands (NMG) over time.

For this analysis, the mammary glands of a mouse are divided into six regions which are symmetric (left vs. right). They are regions 1 to 6 starting clockwise from the left thorax region of a mouse: two regions in thorax, two in inguinal regions and two at the rear end of its body. The following figures show the symmetric comparison of averaged NMG/heart ratio WITHOUT depth correction vs. time. The figures indicate that:

a. The ratios symmetrically match well, ie. NMG1 and 6, 2 and 5, and 3 and 4.

b. NMGs in all regions are saturated at a low level. In more detail, NMGs in inguinal and rear region have the same level of saturation. However, NMGs in thorax regions saturated at a level increased roughly by a factor 1.4. They also accumulate iodine slightly faster than others.

c. Inguinal and rear NMGs are the same in iodine uptake. However, thorax NMGs differ in both speed and level of saturation..

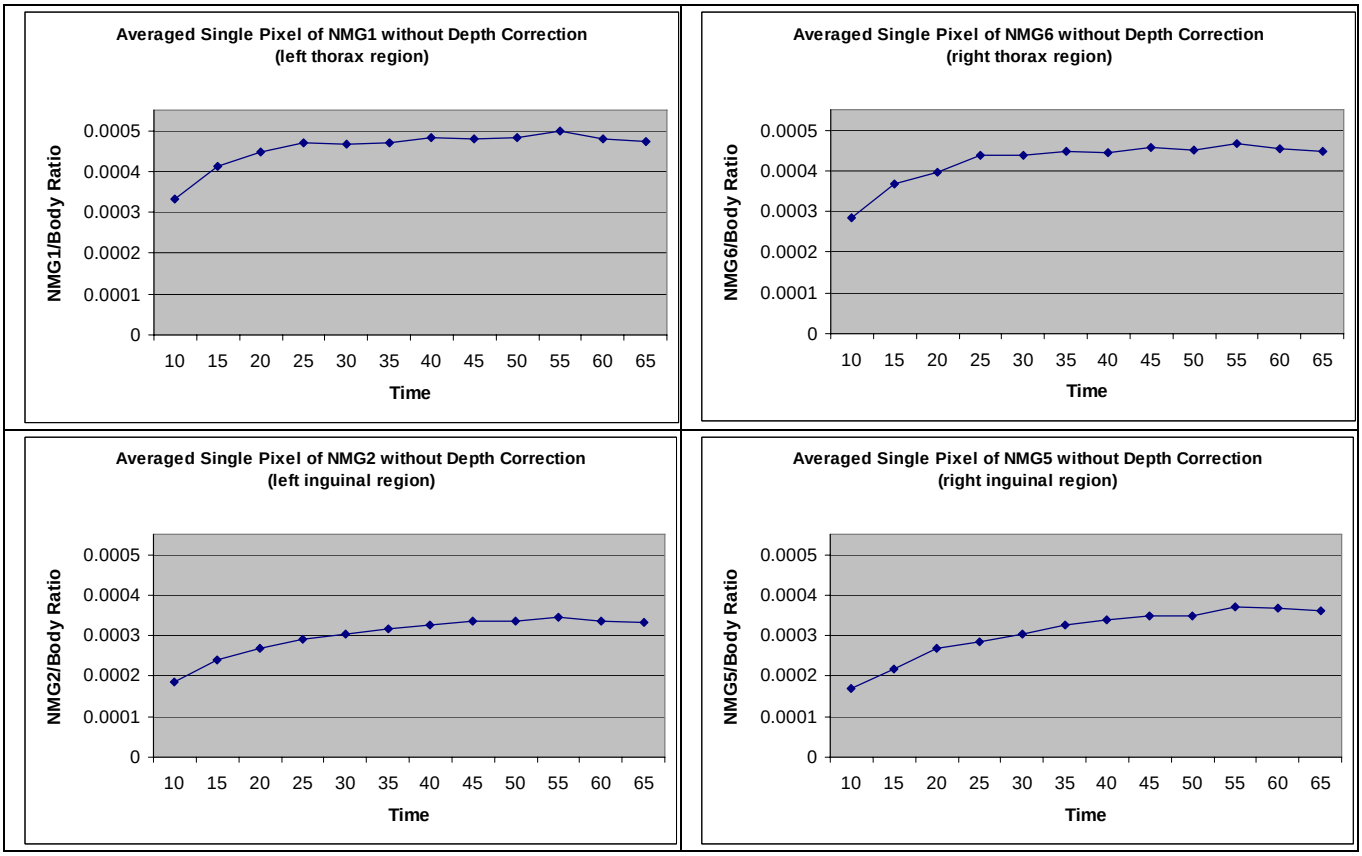

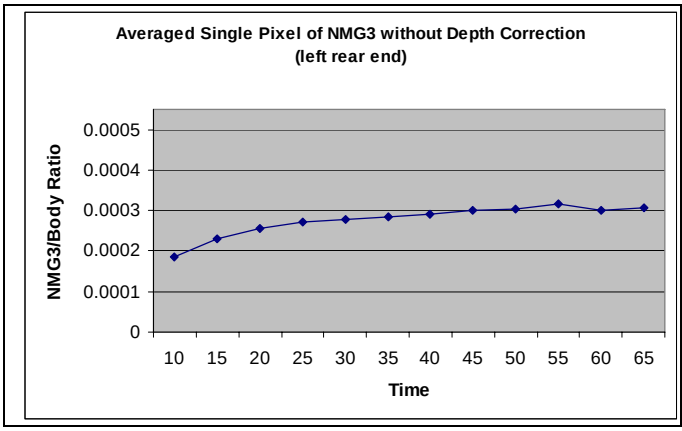

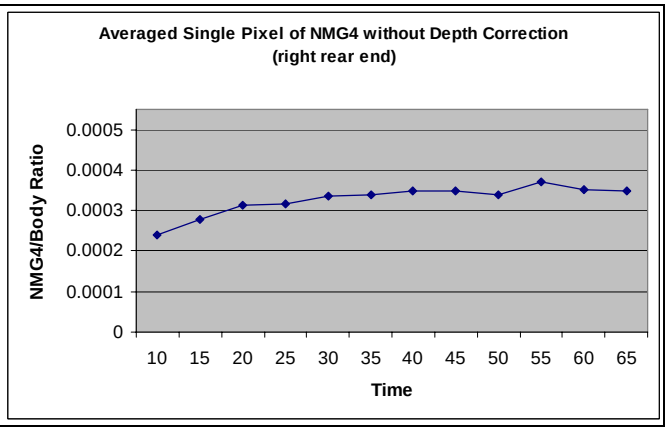

10. Thorax Tumor Comparison

Based on the result of item 9 that NMGs in thorax region take up more isotope than other NMGs and the fact that 45 of 59 tumors are thorax tumors, analysis was performed excluding the 14 inguinal tumors and simply comparing the thorax tumors. The following comparison is based on the averaged single pixel of the hottest region (a 3x3 ROI) in the tumor WITHOUT depth correction. The figures display some interesting points:

a. The left column of figures explicitly suggests the same thing as item 5 does:
   i. The tumors in each group of small, large-2 and advanced size show statistically identical mode of iodine uptake in speed or saturated level.
   ii. However, median and large-1 tumors display two modes of iodine uptake with different speed and saturated level, which is especially clearly represented by median-2 and median-3 tumors. Actually small-3 tumors already start to show large variation in iodine uptake.

b. The right column of figures is the averaged data of each mode of tumor group on the left. Let the dark blue and pink curves on the right represent Mode 1 and Mode 2 tumors respectively. (Please note: There are totally only 4 large-2 and advanced tumors. Since they were rather big tumors, these were combined into one group.)
   iii. All mode-1 curves suggest the corresponding group of tumors are easily saturated at a low level of iodine uptake at first and then start to sluggishly fall later in the first hour.
   iv. Mode-2 curves display some variety. The mode-2 curves of median-1 and median-2 tumors indicate they are more energetic in taking up iodine than their corresponding mode-1 tumors. However, it's not the same case for median-3 and large-1 tumors. Their mode-2 curves show the uptake of iodine saturated faster and becomes somewhat inactive after that.

c. There appear to be two modes of MMTV thorax tumors taking up iodine with difference in both speed and amount. Such division is visible when tumors develop to a certain stage. Mode-2 tumors display more variation.

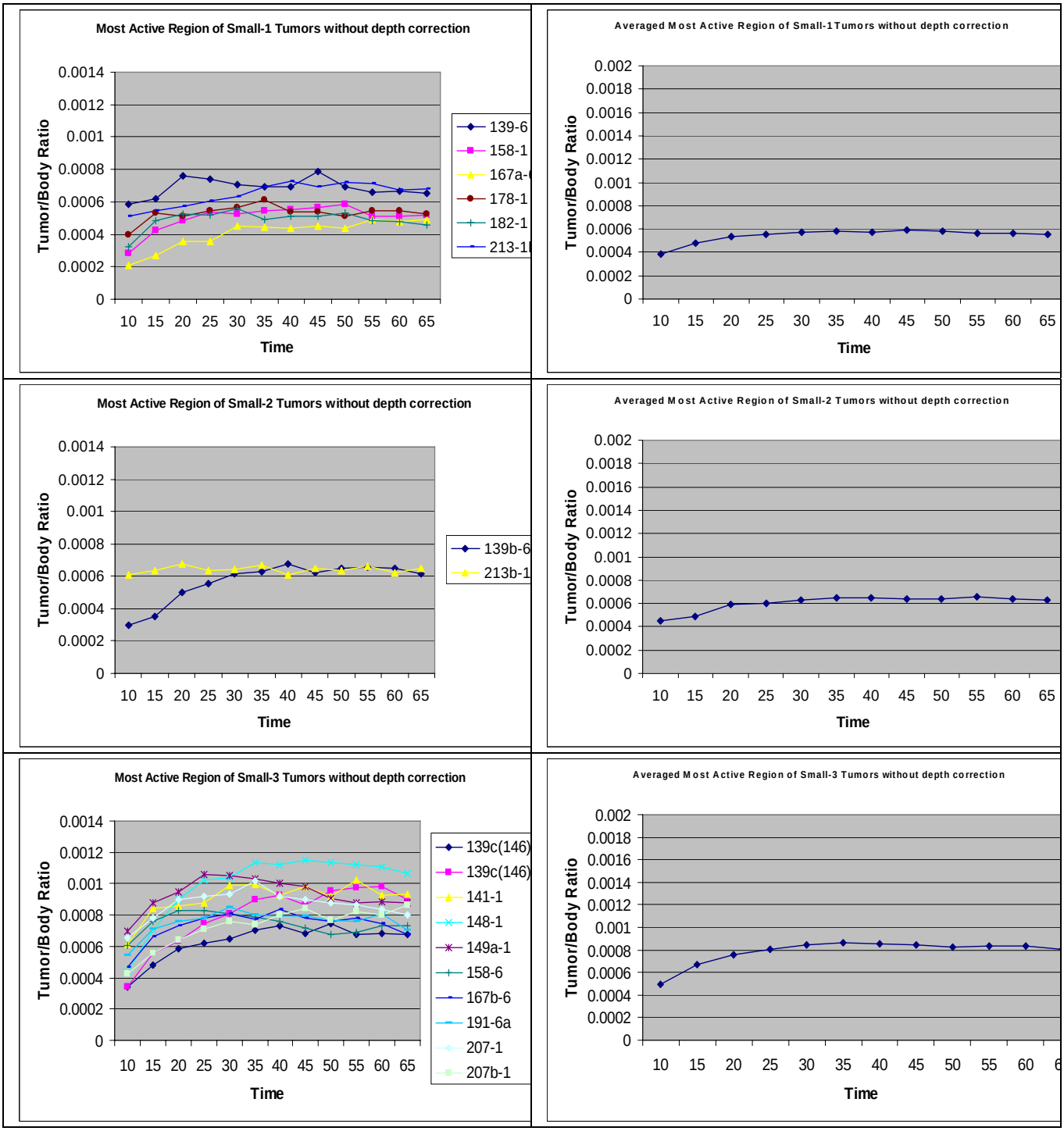
Most Active Region of Small-1 Tumors without depth correction
Tumor/Body Ratio
Time
139-6
158-1
167a-
178-1
182-1
213-1
Averaged Most Active Region of Small-1 Tumors without depth correction
Tumor/Body Ratio
Time
Most Active Region of Small-2 Tumors without depth correction
Tumor/Body Ratio
Time
139b-6
213b-1
Averaged Most Active Region of Small-2 Tumors without depth correction
Tumor/Body Ratio
Time
Most Active Region of Small-3 Tumors without depth correction
Tumor/Body Ratio
Time
139c(146)
139c(146)
141-1
148-1
149a-1
158-6
167b-6
191-6a
207-1
207b-1
Averaged Most Active Region of Small-3 Tumors without depth correction
Tumor/Body Ratio
Time

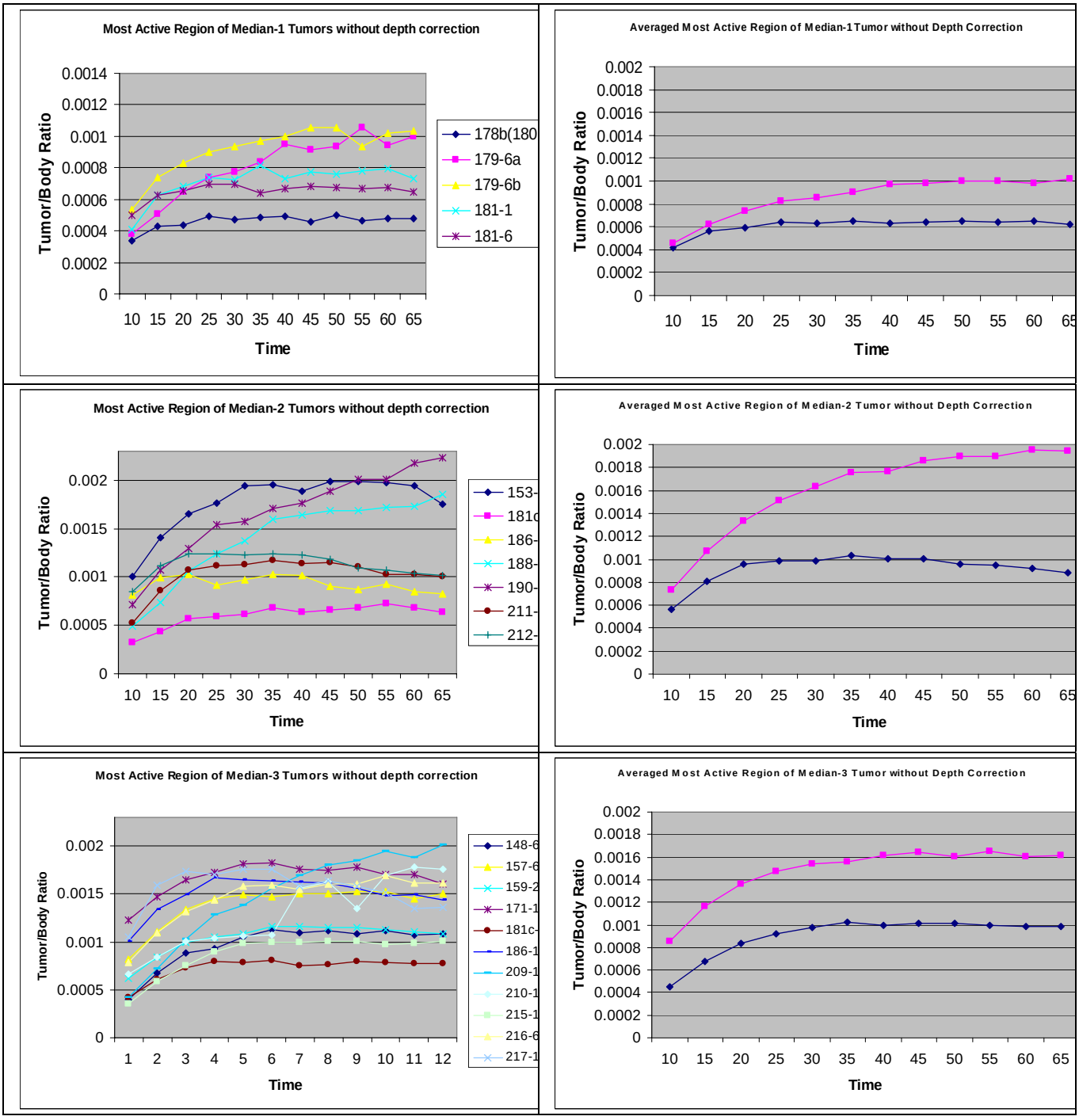
Most Active Region of Median-1 Tumors without depth correction
Tumor/Body Ratio
Time
178b(180
179-6a
179-6b
181-1
181-6
Averaged Most Active Region of Median-1 Tumor without Depth Correction
Tumor/Body Ratio
Time
Most Active Region of Median-2 Tumors without depth correction
Tumor/Body Ratio
Time
153-
181c
186-
188-
190-
211-
212-
Averaged Most Active Region of Median-2 Tumor without Depth Correction
Tumor/Body Ratio
Time
Most Active Region of Median-3 Tumors without depth correction
Tumor/Body Ratio
Time
148-6
157-6
159-2
171-1
181c-
186-1
209-1
210-1
215-1
216-6
217-1
Averaged Most Active Region of Median-3 Tumor without Depth Correction
Tumor/Body Ratio
Time

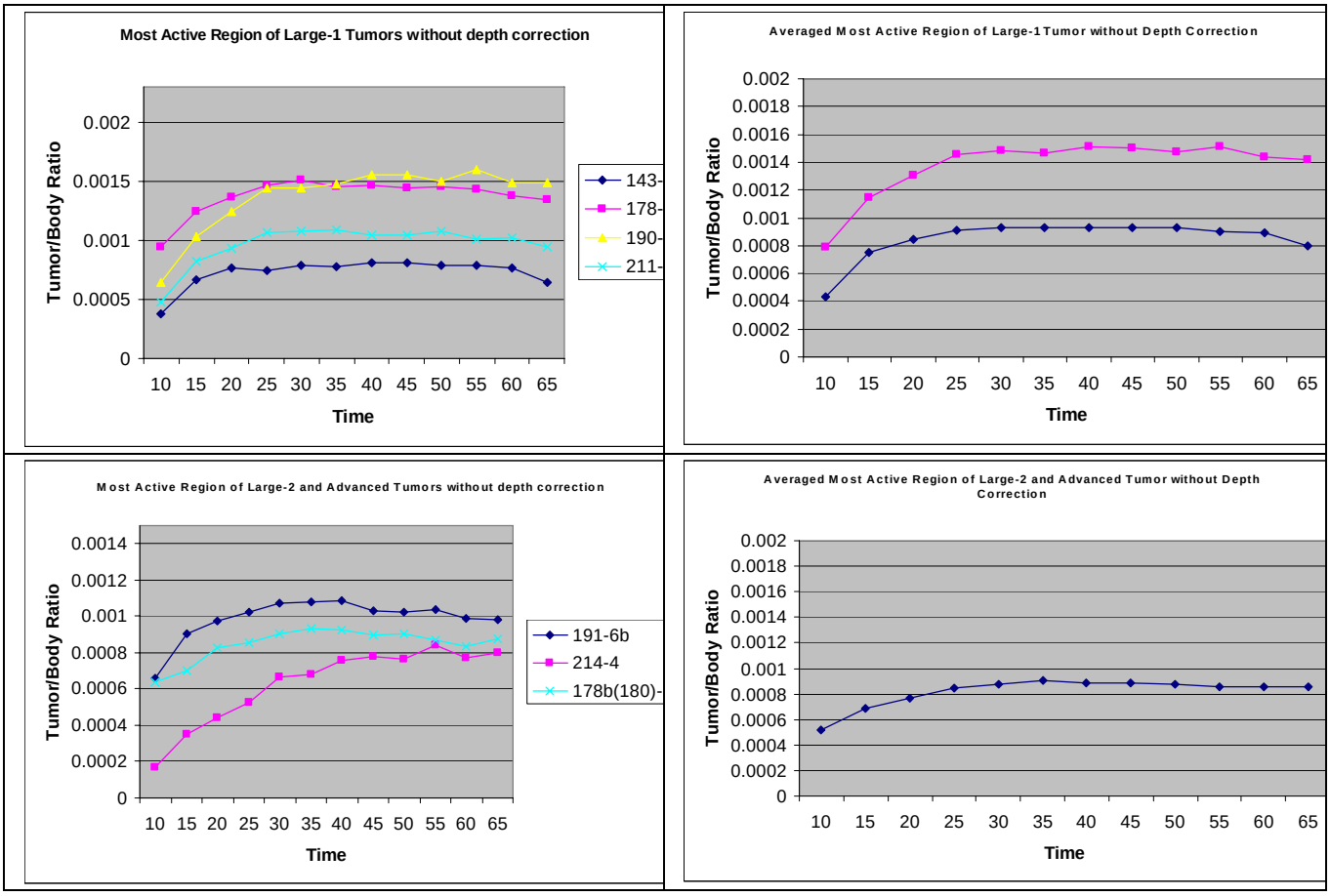

11. Overall analysis of the suitability of NaI for tumor imaging.

To address this problem, it is necessary to determine if the total amount of iodine accumulated in a whole tumor is sufficient for imaging and distinguishable from other tissues. I decided to use the data of Tumor_Outer ROI which is used to cover the whole tumor as much as possible. Its size is variable corresponding to the tumor size. Its shape is always rectangular and, therefore, may include unwanted tissues nearby tumors and cause variable errors. But since the major part will be tumor, I think comparison based on the data is acceptable. I also used the data of a fixed full-size ROI (3x3 pixels) of heart and normal mammary glands as references. Two questions need to be determined:

a. Is the amount of iodine in a whole tumor more than in the blood flow passing through heart?

b. Is it possible that a normal mammary gland is mistaken for an early-stage tumor?

The bottom-right curves of comparison of averaged full-size ROI of tumor, heart and NMG show that, overall, tumors are hotter than heart and NMGs. It may suggest that NaI is good for tumor detection. However, when we look at the individual curves of raw data carefully (first three curves), we found both a few of tumors and a few of NMGs entered the range of heart. (Please note that the first three curves were set to the same maximum scale which caused most tumor curves out of the figure.) That means we cannot tell if those tumors were tumors or normal mammary glands. Our data specifically shows that those tumors physically determined were actually the smallest tumors we had (see the mouse pictures following the curves). Our conclusion is that NaI is good for imaging a tumor developed to certain stage. However, it's not good enough for detecting a tumor in its earliest stage.

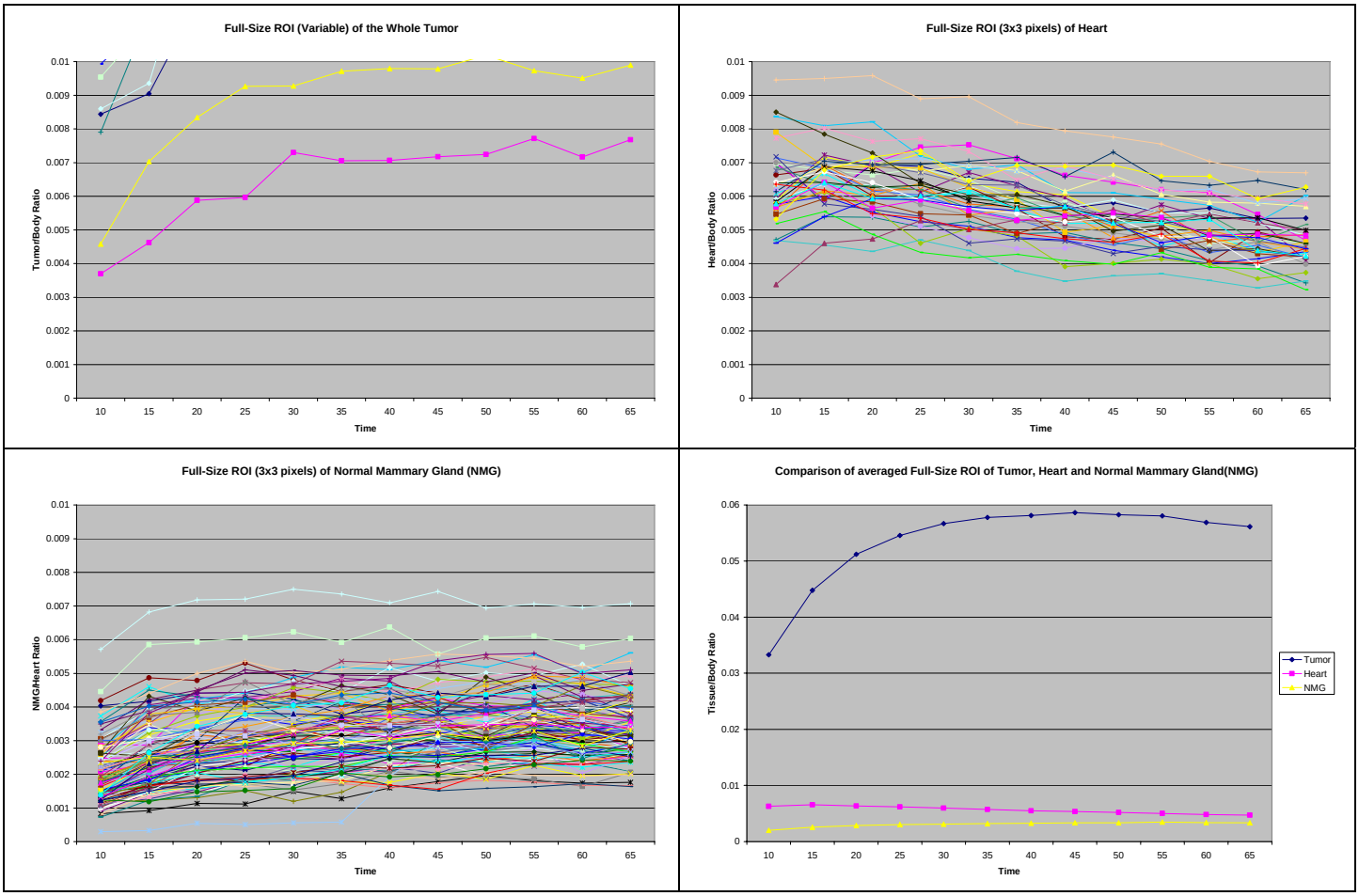
Full-Size ROI (Variable) of the Whole Tumor
Tumor/Body Ratio
Time
Full-Size ROI (3x3 pixels) of Heart
Heart/Body Ratio
Time
Full-Size ROI (3x3 pixels) of Normal Mammary Gland (NMG)
NMG/Heart Ratio
Time
Comparison of averaged Full-Size ROI of Tumor, Heart and Normal Mammary Gland(NMG)
Tissue/Body Ratio
Time
Tumor
Heart
NMG

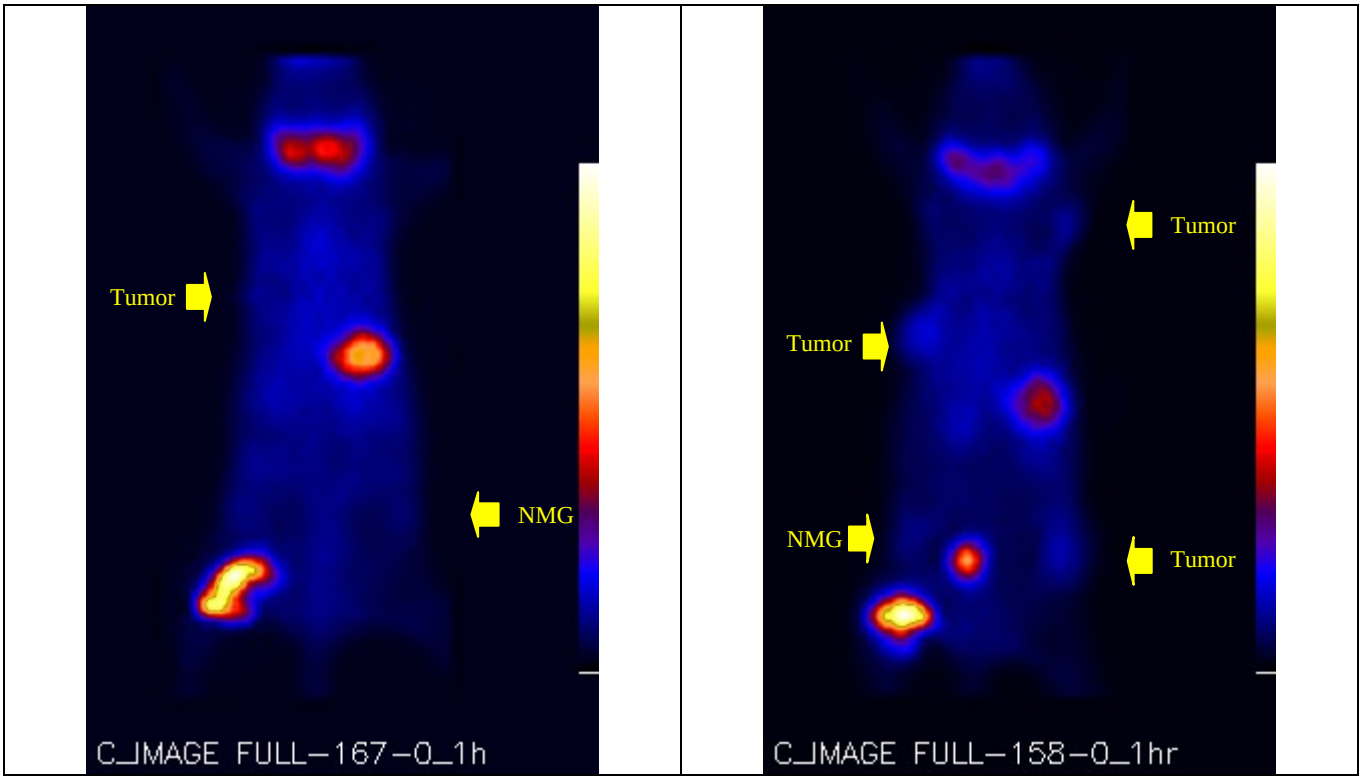

Work conducted using I-125 labeled ligands to image mammary tumors in MMTV tumor animals:

12. **Imaging with VEGF, TGF-alpha, and estradiol**
    I n addition to using I-125 NaI for imaging mammary tumors, three additional I-125 labeled compounds were used: vascular endothelial growth factor, transforming growth factor alpha, and estradiol. Each of these were used on three different mice with tumors at various stages, however none of these ligands were able to effectively and reliably detect mammary tumors to any significant degree.

KEY RESEARCH ACCOMPLISHMENTS

- Although initially promising, the use of I-125 labeled vascular endothelial growth factor, transforming growth factor-alpha, and estradiol to image mammary tumors did not prove to be promising. These compounds did not provide clear, unambiguous, and useful images for very early detection or for even later staged tumors.

- The use of I-125 sodium iodide provided consistently promising images of developing tumors and has potential as a diagnostic and prognostic tool for mammary tumors.

- Our research also suggests a number of hypotheses to be tested. For example, based upon our data, we hypothesize that the presence of a tumor may suppress I-125 NaI uptake in normal mammary glands. If further testing supports this contention, this could have diagnostic potential.

- Our data suggest that I-125 NaI is particularly suitable for determining the heterogeneity within tumors, as well as their stage of development base upon this heterogeneity.

- Our data show that tumors fall into two classes based upon their distinct modes of uptake of I-125 NaI; these different modes may be predictive of the tumor's metastatic potential or aggressiveness.

REPORTABLE OUTCOMES

Manuscripts:

The work conducted through this DOD grant substantially contributed to this manuscript: Margaret S. Saha, corresponding author:

Hammond, W., Bradley, E., Welsh, R., Qian, J., Weisenberger, A., Smith, M., Majewski, S., Saha, M.S., "A Gamma Camera Re-evaluation of Potassium Iodide Blocking Efficiency in Mice," (Status: currently in revision for Health Physics)

Presentations of Graduate Student (Assisting with the Project:):

2006 Academy of Molecular Imaging Annual Conference, March 25-29, 2006
A compact small-animal imaging system incorporating parallel-hole SPECT and multipinhole standard/helical SPECT

Jianguo Qian, Eric L.Bradley, Stan Majewski, Vladimir Popov, Margaret S. Saha, Mark F. Smith, Andrew G. Weisenberger, Robert E. Welsh, and Randolph Wojcik.

We have incorporated multipinhole helical (and ordinary) single photon emission computed tomography (SPECT) in our parallel-hole SPECT imaging system. Previous efforts have demonstrated the utility of parallel-hole SPECT with this system based on two detectors incorporating Hamamatsu R3292 PSPMTs. Recent expansion with a "mousesized" detector incorporating a pair of 2"x2" Hamamatsu H8500 modules enhanced the system further. To address limitations in spatial resolution of our parallel-hole detectors and the sensitivity of our detectors with single-pinhole collimators we have tested a combination of multipinhole and helical SPECT with enlarged field of

view and enhanced resolution and sensitivity. The multipinhole SPECT system is based on the 110mm circular
detector equipped with pixellated (1x1x5mm3/pixel) NaI(Tl) scintillator on a rotating gantry. A helical orbit was effected by adding a rack providing movement of the animal along the axis of rotation of the gantry. The system is capable of organ-specific multipinhole SPECT or whole-body multipinhole helical SPECT. Features are compared among the various modes based on phantom studies.

2006 Users Workshop and Annual Meeting at Jefferson Lab, June 12-14, 2006
A Compact System for Small Animal Nuclear Imaging
Jianguo Qian, Eric L.Bradley, Stan Majewski, Vladimir Popov, Margaret S. Saha,
Mark F. Smith, Andrew G. Weisenberge2, and Robert E. Welsh

Single photon emission computed tomography (SPECT) is now a well established imaging technique. It has shown great promise in small animal imaging for biological studies. Previously, we have demonstrated the utility of parallel-hole SPECT with a compact system based on two detectors incorporating Hamamatsu R3292 position sensitive photomultiplier tubes (PSPMTs). We have recently enhanced the system with a compact "mousesized" detector incorporating a pair of 2"x2" Hamamatsu H8500 PSPMTs. To further address limitations in spatial resolution of the parallel-hole detectors and the sensitivity of detectors with single-pinhole collimators we have expanded the system to include a combination of multipinhole and helical SPECT with an enlarged field of view and enhanced resolution and sensitivity. The multipinhole SPECT system is based on the 110 mm circular detector equipped with pixellated (1x1x5 mm3/pixel) NaI(Tl) scintillator on a rotating gantry. A helical orbit for rotation of the detector about the animal has been accomplished by adding a rack providing movement of the animal along the axis of rotation of the gantry. Features are compared among the various modes of the system based on studies with radioactive phantoms.

Upcoming meeting:
2006 Nuclear Science Symposium, Medical Imaging Conference and 15th International Room Temperature Semiconductor Detector Workshop, October 29 – Nov. 4, 2006
A Multi-Function Compact Small-Animal Imaging System Incorporating Multipinhole Standard and Helical SPECT and Parallel-hole SPECT
Jianguo Qian, *Student Member, IEEE*, Eric L. Bradley, Stan Majewski, Vladimir Popov, Margaret S. Saha, *Member, IEEE*, Mark F. Smith, *Member, IEEE*, Andrew G. Weisenberger and Robert E. Welsh

A small-animal imaging system suitable for SPECT imaging and multipinhole standard/helical SPECT has been designed and constructed. Copper- beryllium parallelhole collimators suitable for imaging the ~35 kev photons from the decay of I-125 have been built and installed to achieve better reconstructed resolution and to reduce imaging time on our dual-detector array. To further address the limitations in the resolution of parallel-hole SPECT and the sensitivity and limited field of view of single-pinhole SPECT, we have incorporated multipinhole standard/helical SPECT in addition to expanding parallel-hole SPECT capabilities. The pinhole SPECT system is based on a 110 mm circular detector equipped with pixellated NaI(Tl) scintillator (1x1x5mm3/pixel). The helical trajectory is accomplished by two stepping motors controlling the rotation of the detector-support gantry and displacement of the animal bed along the axis of rotation of the gantry. Results obtained in SPECT studies of various phantoms show an enlarged field of view, enhanced resolution and improved sensitivity over our earlier results. In particular, improved spatial resolution is obtained with the helical pinhole SPECT. Pinhole collimators with one, three and five 1 mm diameter pinholes have been used in these tests. Spatial resolution of 1.26 mm, 1.43 mm and 1.55 mm have been obtained respectively with those collimators.

CONCLUSION

Overall, the research conducted during the past year has indicated that the use of I-125 labeled NaI has significant potential for the early diagnosis and the potential prognosis for mammary tumors. Uptake of the radiolabel is significantly higher in all tumors than in background tissue, making the tumors visible non-invasively. Moreover, as seen from the images present above, the label is able to display the different types and physiology of the tumors and to reveal their considerable heterogeneity – all non-invasively. This research is of obviously importance and significance to the broader community and to the general public because of the need to develop more non-invasive methods of detecting tumors and providing reasonable and accurate prognoses. Moreover, these non-invasive techniques must employ minimal side effects. The very sensitive detector system we have developed for mammy imaging in small mammals allows for a very low level of radioactive material, in the range of 10 to 100 fold lower than in other imaging systems. However, additional work must be performed. First it will be important to test the utility of I-125 labeled NaI in other model systems as well to determine if our findings can be extended to a variety of tumors. Secondly, future work will include a careful molecular analysis of the tumors and correlation of these data with the imaging and physiological data. Thirdly, hypotheses generated from our data (e.g. the possible suppression of NaI uptake in mammary glands in mice bearing tumors) will be tested to determine potentially novel non-invasive imaging strategies that could be of use with novel therapies (Dadachova et al, 2005; Dwyer et al., 2005; Kogai et al., 2004; Wapnir et al., 2004).

REFERENCES

Cho JY. (2002). A transporter gene (sodium iodide symporter) for dual purposes in gene therapy: imaiging and therapy. Curr Gene Ther. 2(4):393-402.

Chung JK. (2003). Sodium iodide symporter: its role in nuclear medicine. J Nucl Med. 43(9):1188-200.

Dadachova E, Carrasco N. (2004). The Na/I symporter (NIS): imaging and therapeutic applications. Semin Nucl Med. 34(1):23-31

Dadachova E, Nguyen A, Lin EY, Gnatovskiy L, Lu P, Pollard JW. (2005). Treatment with rhenium-188-perrhenate and iodine-131 of NIS-expressing mammary cancer in a mouse model remarkably inhibited tumor growth. Nucl Med Biol. 2005 Oct;32(7):695-700

Dadachova E, Zuckier LS. (2003). Overlooked contributions on sodium iodide symporter. J Nucl Med. 44(10):1707.

Dwyer RM, Bergert ER, O'Connor MK, Gendler SJ, Morris JC. (2005). In vivo radioiodide imaging and treatment of breast cancer xenografts after MUC1-driven expression of the sodium iodide symporter. Clin Cancer Res.11(4):1483-9.

Kogai T, Kanamoto Y, Che LH, Taki K, Moatamed F, Schultz JJ, Brent GA. (2004). Systemic retinoic acid treatment induces sodium/iodide symporter expression and radioiodide uptake in mouse breast cancer models. Cancer Res. 64(1):415-22.

Moon DH, Lee SJ, Park KY, Park KK, Ahn SH, Pai MS, Chang H, Lee HK, Ahn IM. (2001). Correlation between 99mTc-pertechnetate uptakes and expressions of human sodium iodide symporter gene in breast tumor tissues. Nucl Med Biol. 28(7):829-34.

Wapnir IL, Goris M, Yudd A, Dohan O, Adelman D, Nowels K, Carrasco N. (2004). The Na+/I- symporter mediates iodide uptake in breast cancer metastases and can be selectively down-regulated in the thyroid Clin Cancer Res. 10(13):4294-302.